



# A phase-field-based lattice Boltzmann model for multiphase flows involving $N$ immiscible incompressible fluids

Cite as: Phys. Fluids **34**, 023311 (2022); <https://doi.org/10.1063/5.0078507>

Submitted: 13 November 2021 • Accepted: 21 January 2022 • Published Online: 08 February 2022

Xiaolei Yuan (袁晓垒),  Baochang Shi (施保昌),  Chengjie Zhan (湛承杰), et al.



View Online



Export Citation



CrossMark



Author Services

**English Language Editing**

High-quality assistance from subject specialists

LEARN MORE



# A phase-field-based lattice Boltzmann model for multiphase flows involving $N$ immiscible incompressible fluids

Cite as: Phys. Fluids **34**, 023311 (2022); doi: 10.1063/5.0078507

Submitted: 13 November 2021 · Accepted: 21 January 2022 ·

Published Online: 8 February 2022



View Online



Export Citation



CrossMark

Xiaolei Yuan (袁晓垒),<sup>1,2</sup> Baochang Shi (施保昌),<sup>3,4</sup>  Chengjie Zhan (湛承杰),<sup>3,4</sup>  and Zhenhua Chai (柴振华)<sup>3,4,a)</sup> 

## AFFILIATIONS

<sup>1</sup>College of Mathematics and Information Science, Hebei University, Baoding 071002, China

<sup>2</sup>Hebei Key Laboratory of Machine Learning and Computational Intelligence, Hebei University, Baoding 071002, China

<sup>3</sup>School of Mathematics and Statistics, Huazhong University of Science and Technology, Wuhan 430074, China

<sup>4</sup>Hubei Key Laboratory of Engineering Modeling and Scientific Computing, Huazhong University of Science and Technology, Wuhan 430074, China

<sup>a)</sup>Author to whom correspondence should be addressed: [hustczh@hust.edu.cn](mailto:hustczh@hust.edu.cn)

## ABSTRACT

In this work, an efficient and accurate lattice Boltzmann (LB) model is developed based on phase-field theory to study multiphase flows involving  $N$  ( $N \geq 2$ ) immiscible incompressible fluids. In this model, a reduction-consistent physical formulation including a volume-fraction-dependent mobility in the Cahn–Hilliard (C–H) equations is adopted. Usually, the effect of cross-diffusion makes it difficult to solve such equations directly with the classic LB method. To avoid requiring a special treatment on the cross-diffusion terms of the chemical potential gradients, the proposed LB model introduces some non-diagonal collision operators. In addition, the proper auxiliary source terms are constructed to ensure the correct macroscopic equations. Through a direct Taylor expansion, the C–H equations are recovered from the present LB model. Finally, four classical problems including static droplets, the spreading of a liquid lens between two phases, the Kelvin–Helmholtz instability, and the dynamics of droplets in a four-phase system are used to demonstrate the capability of the LB model. The numerical results show that the present model satisfies the reduction-consistent property and produces physically accurate results.

Published under an exclusive license by AIP Publishing. <https://doi.org/10.1063/5.0078507>

## I. INTRODUCTION

Multiphase flows consisting of  $N$  ( $N \geq 2$ ) immiscible incompressible fluids, also referred to as  $N$ -phase flows, frequently arise in nature and engineering applications, such as enhanced oil recovery,<sup>1–3</sup> emulsion formation,<sup>4–7</sup> and rain drops. As an important research tool, the numerical simulation is increasingly popular in the study of these complex flow problems. However, due to the complexity of the moving interface and its topological changes, the numerical simulation of multiphase flows consisting of  $N$  immiscible incompressible fluids remains a challenging task, especially when  $N$  is relatively large.

To date, several popular numerical methods have been developed for multiphase flows, including the volume of fluid method,<sup>8,9</sup> level set method,<sup>10,11</sup> front tracking method,<sup>12</sup> and phase field method.<sup>3,13–18</sup> These methods can be roughly divided into sharp interface (SI) and diffuse interface (DI) approaches. In the SI approach, the thickness of the interface between different phases is zero, which causes physical quantities such as the fluid density and viscosity to jump on either side

of the interface. However, in the DI approach, the thickness of the interface between the two immiscible phases is assumed to be non-zero, and different phases can be characterized by phase variables that vary continuously across thin interfacial layers.

As one of the DI methods, the lattice Boltzmann (LB) method has achieved great success in the simulation of multiphase flows<sup>7,19–22</sup> owing to its simplicity in coding, scalability on parallel computers, and ability to deal with complex geometries. Based on different physical perspectives, the existing LB models for multiphase flows can be classified into four categories: the color-gradient model,<sup>23</sup> the pseudo-potential model,<sup>24</sup> the free-energy model,<sup>25</sup> and the phase-field-based model.<sup>26–32</sup> These models have gained great success in dealing with multiphase flow problems. However, most of the above-mentioned LB models are limited to two-phase flows. Recently, they have been extended to three-phase problems and are sometimes applicable to cases with more than three phases.<sup>7,33–44,58</sup> We must emphasize that these LB models are largely focused on three-phase flows, and only

very few studies have considered multiphase flows involving four or more immiscible incompressible fluids. In fact, it is difficult to generalize the three-phase models to four or more fluid phases, because the number of pairwise surface tensions for  $N \geq 4$  is greater than the number of phase-specific surface-tension coefficients, which leads to an overdetermined system.<sup>2</sup> In the four LB models, the one based on phase-field theory has a clear physical background and a simple model structure, making it highly suitable for numerical simulations. For these reasons, this work focuses on the phase-field-based LB model for multiphase flows involving  $N$  ( $N \geq 4$ ) immiscible incompressible fluids.

Based on the Cahn–Hilliard (C–H) phase-field theory,<sup>45</sup> Zheng *et al.*<sup>46</sup> developed an LB model for  $N$  ( $N \geq 2$ ) immiscible incompressible fluids, in which the mobility between phases  $i$  and  $j$  ( $m_{ij}$ ) is a constant. However, Dong<sup>45</sup> pointed out that, to satisfy the reduction-consistent property, the mobility should be variable-dependent. Here, the reduction-consistent property means that if  $K$  fluids ( $1 \leq K \leq N - 1$ ) are absent from the  $N$ -phase system, the  $N$ -phase system reduces exactly to the  $(N - K)$ -phase system formed by those  $(N - K)$  fluids. As  $m_{ij}$  is a function of  $c_i$ , it is difficult to construct a standard LB model to solve this cross-diffusion system. To solve the problem, Zheng *et al.*<sup>47</sup> proposed a reduction-consistent C–H theory-based LB model for  $N$  immiscible incompressible fluids by introducing a source term containing a gradient term of the chemical potential. However, their model cannot derive the C–H equations correctly. Yuan *et al.*<sup>48</sup> proposed an efficient and alternative LB model for simulating immiscible incompressible  $N$ -phase flows ( $N \geq 2$ ), but this cannot guarantee the reduction-consistent property theoretically.

In general, due to the complexity of multiphase flows involving  $N$  ( $N \geq 2$ ) immiscible incompressible fluids, there are few studies on the phase-field-based LB modeling and numerical simulation for this problem at present, and further development is needed. In view of this, our main purpose is to develop an efficient and accurate lattice Boltzmann (LB) model based on phase-field theory for  $N$ -phase flows. In the present work, inspired by Refs. 49 and 50, where the coupling effects in the cross-diffusion system are reflected through corresponding cross-collision terms in the evolution equation, we develop a C–H theory-based LB model for multiphase flows involving  $N$  ( $N \geq 2$ ) immiscible incompressible fluids, and the reduction-consistent property is satisfied. Different from the previous models,<sup>46–48</sup> in the present model, some non-diagonal collision operators are introduced to model the cross-diffusion terms in the coupled system. Additionally, the proper auxiliary source terms are constructed to recover the macroscopic equations correctly without special treatments for the gradient terms of the chemical potential. To prevent the relaxation matrix from becoming singular, an adjustable matrix is incorporated into the model.

The remainder of this paper is organized as follows. In Sec. II, the physical formulation for the  $N$ -phase immiscible incompressible fluids are presented, and then a phase-field-based LB model is developed in Sec. III. Section IV presents the results of simulations conducted to test the present  $N$ -phase LB model. Finally, the conclusions to this study are summarized in Sec. V.

## II. PHYSICAL FORMULATION FOR THE $N$ -PHASE MIXTURE

### A. Cahn–Hilliard equations for the phase field

In the phase-field theory for multiphase flows of  $N$  immiscible incompressible fluids, the thermodynamic behavior can be described

by a free-energy density defined as a function of the volume fraction  $c_i$  ( $0 \leq c_i \leq 1$ )<sup>45,48</sup>

$$W(\vec{c}, \nabla \vec{c}) = \sum_{i,j=1}^N \frac{l_{ij}}{2} \nabla c_i \cdot \nabla c_j + H(\vec{c}), \quad (1)$$

where  $\vec{c} = (c_1, c_2, \dots, c_N)$  and  $c_i$  ( $1 \leq i \leq N$ ) is the volume fraction of fluid  $i$  within the mixture;  $\sum_{i=1}^N c_i = 1$ . The constant  $l_{ij}$  ( $1 \leq i, j \leq N$ ) denotes the mixing energy density coefficient, which is related to the interfacial thickness  $D$  of the diffuse interfaces.  $H(\vec{c})$  is a multiwell potential term accounting for the bulk energy, which can be written as<sup>45,46</sup>

$$H(\vec{c}) = \sum_{i,j=1}^N \beta_{ij} [g(c_i) + g(c_j) - g(c_i + c_j)], \quad (2)$$

where  $\beta_{ij}$  is a constant depending on the characteristic interfacial thickness  $D$ . The specific expressions of  $l_{ij}$  and  $\beta_{ij}$  can be given as

$$l_{ij} = -\frac{3D}{4} \sigma_{ij}, \quad \beta_{ij} = \frac{3}{D} \sigma_{ij}, \quad (3)$$

where  $\sigma_{ij}$  is the surface tension between fluid  $i$  and fluid  $j$ , which satisfies the following property:

$$\begin{cases} \sigma_{ij} = \sigma_{ji} > 0, & 1 \leq i \neq j \leq N, \\ \sigma_{ij} = 0, & 1 \leq i = j \leq N. \end{cases} \quad (4)$$

By minimizing the total free-energy density function [Eq. (1)], the chemical potential  $C_i$  can be obtained from the variation of the free energy<sup>31,51</sup>

$$C_i = \frac{\partial W}{\partial c_i} - \nabla \cdot \frac{\partial W}{\partial \nabla c_i}, \quad 1 \leq i \leq N. \quad (5)$$

In the phase-field theory, the diffusion of  $c_i$  is driven by the chemical potential gradient, and the volume fractions are governed by the following C–H equations:<sup>2,45,46</sup>

$$\frac{\partial c_i}{\partial t} + \mathbf{u} \cdot \nabla c_i = \sum_{j=1}^N \nabla \cdot [m_{ij}(\vec{c}) \nabla C_j], \quad 1 \leq i \leq N, \quad (6)$$

where  $\mathbf{u}$  is the fluid velocity and  $m_{ij}$  is referred to as the mobility coefficient. Based on Onsager's reciprocal relation, the mobility matrix  $\mathbf{m} = [m_{ij}]_{N \times N}$  should be symmetric.<sup>45</sup> Furthermore, the mobility matrix satisfies the following relation:

$$\sum_{j=1}^N m_{ij} = \sum_{j=1}^N m_{ji} = 0, \quad 1 \leq i \leq N. \quad (7)$$

For simplicity, the mobility coefficient can be explicitly expressed as<sup>45</sup>

$$\begin{cases} m_{ij} = -m_0 c_i^2 c_j^2, & i \neq j, \\ m_{ii} = -\sum_{j=1, j \neq i}^N m_{ij}, & i = j, \end{cases} \quad (8)$$

where  $m_0$  is a positive constant. It is easy to show that the mobility coefficient  $m_{ij}$  ( $1 \leq i, j \leq N$ ) defined above is symmetric and satisfies

condition (7). Additionally, when the  $i$ th fluid is absent (i.e.,  $c_i = 0$ ), the mobility coefficient related to the  $i$ th fluid is zero.

In addition to the C–H equations for capturing the phase interfaces, the hydrodynamic equations for the flow field are needed. In this work, we consider the following incompressible Navier–Stokes (N–S) equations:<sup>48</sup>

$$\nabla \cdot \mathbf{u} = 0, \quad (9a)$$

$$\frac{\partial(\rho \mathbf{u})}{\partial t} + \nabla \cdot (\rho \mathbf{u} \mathbf{u}) = -\nabla p + \nabla \cdot [\mu(\phi) \mathbf{D}(\mathbf{u})] - \nabla \cdot (\tilde{\mathbf{J}} \mathbf{u}) + \mathbf{F}_s + \mathbf{G}(\mathbf{x}, t), \quad (9b)$$

where  $\rho$  is the density of the mixture,  $p$  denotes the pressure,  $\mu(\phi)$  is the dynamic viscosity,  $\mathbf{D}(\mathbf{u}) = \nabla \mathbf{u} + \nabla \mathbf{u}^T$ , and  $\tilde{\mathbf{J}}$  is the flux, with  $\tilde{\mathbf{J}} = -\sum_{i,j=1}^N \tilde{\rho}_i m_{ij} \nabla C_j$  ( $\tilde{\rho}_i$  is the constant density of the  $i$ th fluid).  $\mathbf{F}_s$  represents the interface force, with  $\mathbf{F}_s = \sum_{j=1}^N C_j \nabla C_j$ , and  $\mathbf{G}(\mathbf{x}, t)$  is an external body force related to position  $\mathbf{x}$  and time  $t$ .

The dynamics of the  $N$ -phase mixture is described by Eqs. (6) and (9). Note that only  $(N - 1)$  expressions in Eq. (6) are independent because of  $\sum_{i=1}^N c_i = 1$  and condition (7). In this model, the mixture density and dynamic viscosity are given by

$$\rho = \sum_{i=1}^N c_i \tilde{\rho}_i, \quad \mu = \sum_{i=1}^N c_i \tilde{\mu}_i, \quad (10)$$

where  $\tilde{\mu}_i$  denotes the constant dynamic viscosity of fluid  $i$ .

### III. LB MODEL FOR MULTIPHASE FLOWS OF $N$ IMMISCIBLE INCOMPRESSIBLE FLUIDS

#### A. LB model for the phase field

As we can see, Eq. (6) describes a typical cross-diffusion system driven by a chemical potential gradient. In the model of Zheng *et al.*,<sup>46</sup> a special treatment of introducing a source term containing a gradient term of the chemical potential is adopted to deal with the cross-diffusion terms. However, this method cannot correctly derive the macroscopic equations. In Ref. 49, Chai *et al.* developed a multiple-relaxation-time LB model for the mass diffusion in multicomponent mixtures. In their model, the coupling effects among different species are reflected through corresponding cross-collision terms in the LB equations. Based on their work, to avoid the need to apply any special treatments to the gradient terms, some non-diagonal collision operators are introduced to model the cross-diffusion terms in the coupled system. The LB equations for the phase field can then be written as

$$f_{k,i}(\mathbf{x} + \mathbf{c}_i \Delta t, t + \Delta t) - f_{k,i}(\mathbf{x}, t) = -\lambda_{ij} [f_{k,j}(\mathbf{x}, t) - f_{k,j}^{eq}(\mathbf{x}, t)] + \Delta t R_{k,i}(\mathbf{x}, t), \quad 1 \leq i \leq N, \quad (11)$$

where  $f_{k,i}(\mathbf{x}, t)$  ( $k = 1, 2, \dots, q - 1$ ,  $q$  is the number of discrete velocity directions) represents the particle distribution function of the volume fraction at position  $\mathbf{x}$  and time  $t$ ,  $f_{k,i}^{eq}(\mathbf{x}, t)$  is the corresponding local equilibrium distribution function,  $R_{k,i}(\mathbf{x}, t)$  is the source term,  $\mathbf{c}_i$  denotes the discrete velocity, and  $\Delta t$  is the time step.  $(\lambda_{ij})$  is an invertible  $N \times N$  relaxation matrix, where  $\lambda_{ii}$  represents the relaxation factor of the  $i$ th fluid itself, and  $\lambda_{ij}$  ( $i \neq j$ ) is the relaxation factor of the intersection between the  $i$ th and  $j$ th fluids.

To obtain the correct macroscopic equations [Eq. (6)], the local equilibrium distribution function  $f_{k,i}^{eq}(\mathbf{x}, t)$  and the source term  $R_{k,i}(\mathbf{x}, t)$  are designed as

$$f_{k,i}^{eq}(\mathbf{x}, t) = \omega_k \left[ c_i + \frac{\mathbf{c}_k \cdot c_i \mathbf{u}}{c_s^2} + \frac{(\mathbf{c}_k \mathbf{c}_k - c_s^2 \mathbf{I}) : (K_{ij} C_j \mathbf{I})}{2c_s^4} \right], \quad 1 \leq i \leq N, \quad (12)$$

$$R_{k,i}(\mathbf{x}, t) = \left( \delta_{ij} - \frac{\lambda_{ij}}{2} \right) \frac{\omega_k \mathbf{c}_k \cdot [\partial_t (c_i \mathbf{u}) + c_s^2 \nabla c_j]}{c_s^2}, \quad 1 \leq i \leq N, \quad (13)$$

where  $\omega_i$  is the weight coefficient and  $(K_{ij})$  is an  $N \times N$  invertible matrix for adjusting the relaxation matrix  $(\lambda_{ij})$ .

In this study, for simplicity and without any loss of generality, we focus on two-dimensional (2D) problems, and adopt the 2D nine-velocity (D2Q9) lattice model.<sup>52</sup> In this lattice model, the weight coefficients, discrete velocities, and lattice sound speed are given by

$$\omega_k = \begin{cases} \frac{4}{9}, & k = 0, \\ \frac{1}{9}, & k = 1 - 4, \\ \frac{1}{36}, & k = 5 - 8, \end{cases} \quad (14a)$$

$$\mathbf{c}_k = \begin{cases} (0, 0), & k = 0, \\ \left( \cos \left[ \frac{(k-1)\pi}{2} \right], \sin \left[ \frac{(k-1)\pi}{2} \right] \right), & k = 1 - 4, \\ \sqrt{2} \left( \cos \left[ \frac{(k-1)\pi}{2} + \frac{\pi}{4} \right], \sin \left[ \frac{(k-1)\pi}{2} + \frac{\pi}{4} \right] \right), & k = 5 - 8, \end{cases} \quad (14b)$$

$$c_s = c/\sqrt{3}, \quad (14c)$$

where  $c = \Delta x/\Delta t$  is the lattice speed with the time step  $\Delta t$  and lattice spacing  $\Delta x$  ( $\Delta x = \Delta t = 1$  is used in the following simulations).

The volume fraction  $c_i$  in the present LB model is obtained by taking the zero-order moment of  $f_{k,i}$ , i.e.,

$$c_i = \sum_k f_{k,i}, \quad 1 \leq i \leq N. \quad (15)$$

#### 1. Direct Taylor expansion analysis of present LB model for the phase field

Direct Taylor expansion analysis is now performed to demonstrate that the present LB model gives the correct governing equations [Eq. (6)]. Applying the Taylor expansion to Eq. (11), we obtain

$$\sum_{l=1}^N \frac{\Delta t^l}{l!} D_k^l f_{k,i} + O(\Delta t^{N+1}) = -\lambda_{ij} f_{k,j}^{ne} + \Delta t R_{k,i}, \quad (16)$$

where  $D_k = \partial_t + \mathbf{c}_k \cdot \nabla$  and  $f_{k,i}^{ne} = f_{k,i} - f_{k,i}^{eq}$  is the non-equilibrium distribution function. From Eq. (16), we have that

$$f_{k,i}^{ne} = O(\Delta t), \quad (17a)$$

$$\sum_{l=1}^{N-1} \frac{\Delta t^l}{l!} D_k^l (f_{k,i}^{eq} + f_{k,i}^{ne}) + \frac{\Delta t^N}{N!} D_k^N f_{k,i}^{eq} = -\lambda_{ij} f_{k,j}^{ne} + \Delta t R_{k,i} + O(\Delta t^{N+1}). \quad (17b)$$

With the help of Eq. (17a), we can obtain the following equations at different orders of  $\Delta t$ :

$$D_k f_{k,i}^{eq} = -\frac{\lambda_{ij}}{\Delta t} f_{k,j}^{ne} + R_{k,i} + O(\Delta t), \quad (18a)$$

$$D_k (f_{k,i}^{eq} + f_{k,i}^{ne}) + \frac{\Delta t}{2} D_k^2 f_{k,i}^{eq} = -\frac{\lambda_{ij}}{\Delta t} f_{k,j}^{ne} + R_{k,i} + O(\Delta t^2). \quad (18b)$$

According to Eq. (18a), we can derive

$$\frac{\Delta t}{2} D_k^2 f_{k,i}^{eq} = -\frac{1}{2} D_k \lambda_{ij} f_{k,j}^{ne} + \frac{\Delta t}{2} D_k R_{k,i} + O(\Delta t^2). \quad (19)$$

Substituting Eq. (19) into Eq. (18b), we have

$$D_k f_{k,i}^{eq} + D_k \left( \delta_{ij} - \frac{\lambda_{ij}}{2} \right) f_{k,j}^{ne} + \frac{\Delta t}{2} D_k R_{k,i} = -\frac{\lambda_{ij}}{\Delta t} f_{k,j}^{ne} + R_{k,i} + O(\Delta t^2). \quad (20)$$

Based on Eqs. (12) and (13), the following moment conditions hold:

$$\sum_k f_{k,i}^{eq} = \sum_k f_{k,i} = c_i, \quad \sum_k \mathbf{c}_k f_{k,i}^{eq} = c_i \mathbf{u}, \quad (21a)$$

$$\sum_k \mathbf{c}_k \mathbf{c}_k f_{k,i}^{eq} = c_s^2 c_i \mathbf{I} + c_s^2 K_{ij} c_j \mathbf{I}, \quad (21b)$$

$$\sum_k R_{k,i} = 0, \quad \sum_k \mathbf{c}_k R_{k,i} = \left( \delta_{ij} - \frac{\lambda_{ij}}{2} \right) (\partial_t c_j \mathbf{u} + c_s^2 \nabla c_j). \quad (21b)$$

Summing Eq. (20) over  $k$  and using the above relations, we obtain

$$\begin{aligned} \partial_t c_i + \nabla \cdot (c_i \mathbf{u}) &= O(\Delta t), \\ \partial_t c_i + \nabla \cdot (c_i \mathbf{u}) + \nabla \cdot \left( \delta_{im} - \frac{\lambda_{im}}{2} \right) \sum_k \mathbf{c}_k f_{k,m}^{ne} \\ &= -\frac{\Delta t}{2} \nabla \cdot \left[ \left( \delta_{ij} - \frac{\lambda_{ij}}{2} \right) (\partial_t c_j \mathbf{u} + c_s^2 \nabla c_j) \right] + O(\Delta t^2), \end{aligned} \quad (22a)$$

where  $\sum_k \mathbf{c}_k f_{k,m}^{ne}$  can be calculated by Eq. (18) as

$$\begin{aligned} \sum_k \mathbf{c}_k f_{k,m}^{ne} &= -\lambda_{mj}^{-1} \Delta t \left[ \partial_t (c_j \mathbf{u}) + c_s^2 \nabla c_j + c_s^2 K_{jp} \nabla C_p \right. \\ &\quad \left. - \left( \delta_{jp} - \frac{\lambda_{jp}}{2} \right) (\partial_t c_p \mathbf{u} + c_s^2 \nabla c_p) \right] + O(\Delta t^2) \\ &= -\lambda_{mj}^{-1} \Delta t \left[ c_s^2 K_{jp} \nabla C_p + \frac{\lambda_{jp}}{2} (\partial_t c_p \mathbf{u} + c_s^2 \nabla c_p) \right] + O(\Delta t^2), \end{aligned} \quad (23)$$

where  $(\lambda_{mj}^{-1})$  represents the inverse matrix of  $(\lambda_{jp})$ . Substituting Eq. (23) into Eq. (22b) gives, and after some manipulations,

$$\partial_t c_i + \nabla \cdot (c_i \mathbf{u}) = \nabla \cdot (m_{ij} \nabla C_j) + O(\Delta t^2), \quad (24)$$

with the relation

$$m_{ij} = \left( \lambda_{ip}^{-1} - \frac{\delta_{ip}}{2} \right) K_{jp} c_s^2 \Delta t. \quad (25)$$

From the above procedure, it is clear that the present LB model correctly recovers Eq. (6) with a truncation error of  $O(\Delta t^2)$ .

## B. LB equation for the flow field

The evolution equation of the LB model for the N-S equations can be expressed as<sup>48,53</sup>

$$\begin{aligned} g_k(\mathbf{x} + \mathbf{c}_k \Delta t, t + \Delta t) - g_k(\mathbf{x}, t) &= -\frac{1}{\tau_g} [g_k(\mathbf{x}, t) - g_k^{eq}(\mathbf{x}, t)] \\ &\quad + \Delta t \left( 1 - \frac{1}{2\tau_g} \right) G_k(\mathbf{x}, t), \end{aligned} \quad (26)$$

where  $g_k(\mathbf{x}, t)$  is the distribution function and  $\tau_g$  is the dimensionless relaxation time, which is related to the kinematic viscosity  $\nu = \mu/\rho = c_s^2(\tau_g - 0.5)\Delta t$ .  $g_k^{eq}(\mathbf{x}, t)$  is the local equilibrium distribution function, which is given by<sup>54</sup>

$$g_k^{eq}(\mathbf{x}, t) = \begin{cases} \rho_0 + \frac{p}{c_s^2}(\omega_k - 1) + \rho s_k(\mathbf{u}), & k = 0, \\ \frac{p}{c_s^2} \omega_k + \rho s_k(\mathbf{u}), & k = 1 - 8, \end{cases} \quad (27)$$

with

$$s_k(\mathbf{u}) = \omega_k \left[ \frac{\mathbf{c}_k \cdot \mathbf{u}}{c_s^2} + \frac{(\mathbf{c}_k \cdot \mathbf{u})^2}{2c_s^4} - \frac{\mathbf{u} \cdot \mathbf{u}}{2c_s^4} \right]. \quad (28)$$

To recover the N-S equations correctly, the force distribution function  $G_i(\mathbf{x}, t)$  is expressed as<sup>48</sup>

$$\begin{aligned} G_k &= \omega_k \left\{ \mathbf{u} \cdot \nabla \rho + \frac{\mathbf{c}_k \cdot \mathbf{F}}{c_s^2} \right. \\ &\quad \left. + \frac{(\mathbf{c}_k \mathbf{c}_k - c_s^2 \mathbf{I}) : \left[ \mathbf{u} \mathbf{F} + \mathbf{F} \mathbf{u} + c_s^2 \mathbf{u} \nabla \rho + c_s^2 (\nabla \rho) \mathbf{u} + \frac{\tilde{\mathbf{J}} \mathbf{u}}{\Delta t (\tau_g - 0.5)} \right]}{2c_s^4} \right\}, \end{aligned} \quad (29)$$

where  $\mathbf{F} = \mathbf{F}_s + \mathbf{G}$  is the forcing term. The macroscopic local fluid velocity  $\mathbf{u}$  and the pressure  $p$  are calculated by<sup>48,54</sup>

$$\rho \mathbf{u} = \sum_k \mathbf{c}_k g_k + 0.5 \Delta t \mathbf{F}, \quad (30)$$

$$p = \frac{c_s^2}{1 - \omega_0} \left[ \sum_{k \neq 0} g_k + \frac{\Delta t}{2} \mathbf{u} \cdot \nabla \rho + \rho s_0(\mathbf{u}) \right]. \quad (31)$$

Note that Chapman–Enskog analysis can be applied to the present LB model for the flow field to derive the N-S equations [Eq. (9)]; readers are referred to Ref. 48 for details. In addition, some special difference schemes are needed to compute the gradient and Laplacian terms in the forcing term  $G_k$ , chemical potentials  $C_p$ , and surface tension  $\mathbf{F}_s$ . Although there are many suitable schemes,<sup>54,55</sup> the following are used in this study:

$$\nabla \zeta(\mathbf{x}, t) = \sum_{k \neq 0} \frac{\omega_k \mathbf{c}_k [\zeta(\mathbf{x} + \mathbf{c}_k \Delta t, t) - \zeta(\mathbf{x} - \mathbf{c}_k \Delta t, t)]}{2c_s^2 \Delta t}, \quad (32a)$$

$$\nabla^2 \zeta(\mathbf{x}, t) = \sum_{k \neq 0} \frac{\omega_k [\zeta(\mathbf{x} + \mathbf{c}_k \Delta t, t) - 2\zeta(\mathbf{x}, t) + \zeta(\mathbf{x} - \mathbf{c}_k \Delta t, t)]}{c_s^2 \Delta t^2}, \quad (32b)$$

where  $\zeta$  is an arbitrary function. According to the Taylor expansion, it can be shown that Eqs. (32a) and (32b) have a second-order



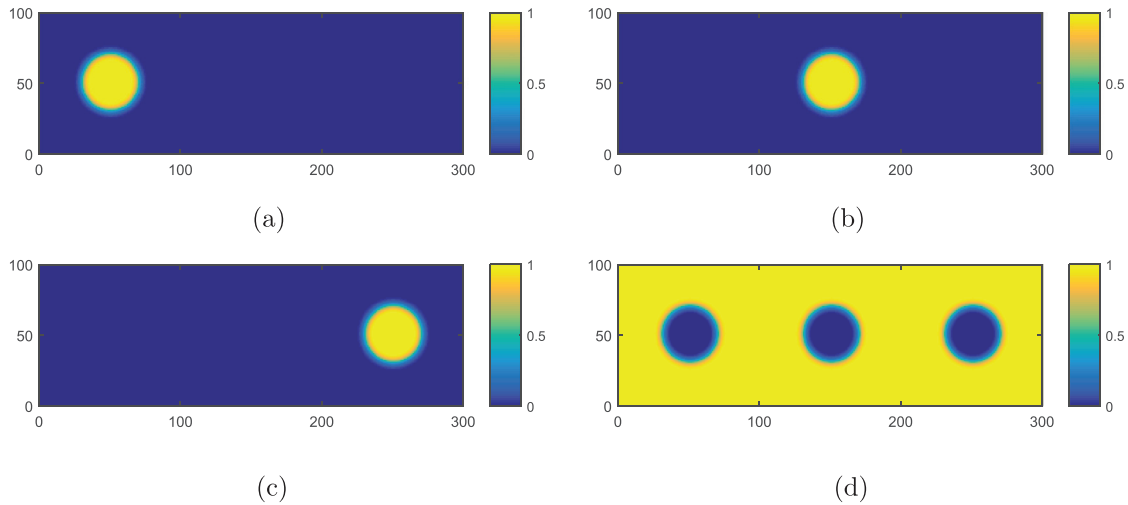


FIG. 1. The steady distributions of the volume fractions obtained by the present LB model: (a)  $c_1$ , (b)  $c_2$ , (c)  $c_3$ , and (d)  $c_4$ .

convergence rate in space. Moreover, this scheme ensures the global mass conservation of an  $N$ -phase system.

#### IV. NUMERICAL SIMULATIONS AND DISCUSSION

In this section, four classical problems are employed to demonstrate the capability of the LB model. These problems cover static droplets, the spreading of a liquid lens between two phases, the Kelvin–Helmholtz (KH) instability, and the dynamics of droplets in a four-phase system. Some detailed comparisons of the present results with the analytical solutions or available data are conducted. Prior to all simulations, grid resolution tests were performed, and the grid sizes adopted for simulations were found to be fine enough to give grid-independent results.

##### A. Static droplets

A benchmark test of static droplets ( $N = 3, 4$ ) is performed to test the present LB model. We first consider the situation consisting of four immiscible incompressible fluids ( $N = 4$ ). Initially, three droplets with radius  $R = 20$  are placed in a computational domain of size  $NX \times NY = 300 \times 100$ , with periodic boundary condition applied at all boundaries. The initial volume fractions are given by

$$c_1(x, y) = 0.5 + 0.5 \tanh \frac{2 \left[ R - \sqrt{(x - x_{c_1})^2 + (y - y_{c_1})^2} \right]}{D}, \quad (33a)$$

$$c_2(x, y) = 0.5 + 0.5 \tanh \frac{2 \left[ R - \sqrt{(x - x_{c_2})^2 + (y - y_{c_2})^2} \right]}{D}, \quad (33b)$$

$$c_3(x, y) = 0.5 + 0.5 \tanh \frac{2 \left[ R - \sqrt{(x - x_{c_3})^2 + (y - y_{c_3})^2} \right]}{D}, \quad (33c)$$

$$c_4(x, y) = 1.0 - c_1(x, y) - c_2(x, y) - c_3(x, y), \quad (33d)$$

where  $(x_{c_1}, y_{c_1})$ ,  $(x_{c_2}, y_{c_2})$ , and  $(x_{c_3}, y_{c_3})$  are the centers of the circular droplets; these are fixed to  $(x_{c_1}, y_{c_1}) = (50, 50)$ ,  $(x_{c_2}, y_{c_2}) = (150, 50)$ ,

and  $(x_{c_3}, y_{c_3}) = (200, 50)$ . In these simulations,  $\rho_1 : \rho_2 : \rho_3 : \rho_4 = 20 : 1 : 10 : 5$ ,  $\tau_g = 0.8$ ,  $\sigma_{ij} = 0.01$  ( $i \neq j$ ),  $m_0 = 0.05$ ,  $D = 3$ , and the relaxation matrix  $\omega_{ip} = \frac{1}{0.503} \delta_{ip}$ . Figure 1 shows the steady distributions of the volume fractions obtained by the present LB model, and it is clear that the model can accurately preserve the profiles of the volume fractions. To provide a quantitative comparison, we also plot the volume fractions along the centerline ( $y = 50$ ,  $0 \leq x \leq 300$ ) in Fig. 2, showing that the numerical results are in good agreement with the analytical solutions.

In addition, we show that the present LB model for  $N$ -phase flows satisfies the reduction-consistent property. To this end, the volume fraction of the third phase in the previous test is set to zero, and we demonstrate that the four-phase model is able to accurately simulate the static droplet problem of three immiscible incompressible fluids. For convenience, the fourth phase in the former case is denoted

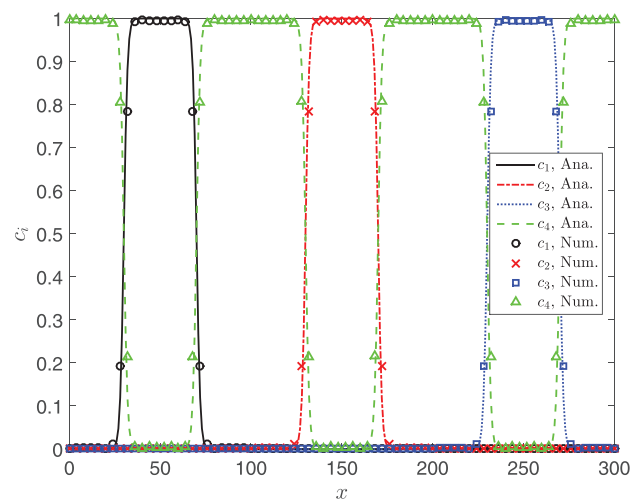


FIG. 2. The profiles of volume fractions along the centerline ( $y = 50$ ,  $0 \leq x \leq 300$ ), where Ana. and Num. denote analytical and numerical results.

as the third phase here. A comparison of the volume fractions obtained from the three-phase model, the four-phase model with one phase removed, and the theoretical solution is shown in Fig. 3. The results of the three-phase model and four-phase model with one phase removed are almost identical, and they are also in good agreement with the theoretical solution. In addition, we also consider two phases (the first and the third phase) removed in the present four-phase LB model, and the results are compared with the theoretical solutions. The results are shown in Fig. 4, where we find that the numerical results of the four-phase model with two phase removed are also in good agreement with the theoretical ones. These results demonstrate that the reduction-consistent property is preserved in the present LB model.

### B. Spreading of a liquid lens

We now test the developed LB model by considering the spreading of a liquid lens. As a classic benchmark problem for three-phase flows, this has been widely investigated in the literature<sup>16,17,56–58</sup> because its theoretical solution is available. In particular, when the effect of gravity is dominant, quantitative relations for the droplet thickness in terms of the other parameters have been developed.<sup>59,60</sup> Here, we compare the numerical results against the Langmuir–de Gennes theory to validate our LB model and demonstrate its capacity to preserve the reduction-consistent property.

We consider a droplet (phase 1) located at the interface between two other immiscible fluids (phases 2 and 3). Under the influence of surface tension, the droplet will form a lens when the system reaches the equilibrium state. According to Neumann's law,<sup>61</sup> the equilibrium contact angle and surface tension are related as follows:

$$\cos(\theta_1) = \frac{\sigma_{12}^2 + \sigma_{23}^2 - \sigma_{13}^2}{2\sigma_{12}\sigma_{23}}, \quad \cos(\theta_2) = \frac{\sigma_{13}^2 + \sigma_{23}^2 - \sigma_{12}^2}{2\sigma_{13}\sigma_{23}}, \quad (34)$$

where  $\theta_i$  ( $i = 1, 2$ ) represents the contact angle. From the schematic shown in Fig. 5, the length  $d$  (the distance between two triple junctions) can be calculated as

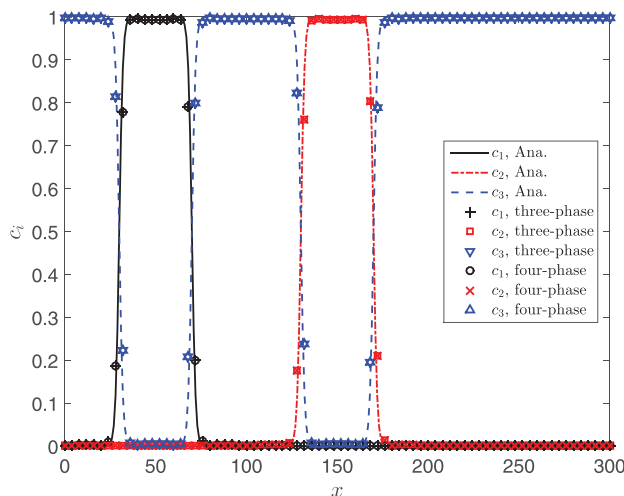


**FIG. 3.** A comparison of volume fractions obtained from the three-phase model, four-phase model with one phase disappeared, and the theoretical solutions along the centerline ( $y = 50$ ,  $0 \leq x \leq 300$ ).

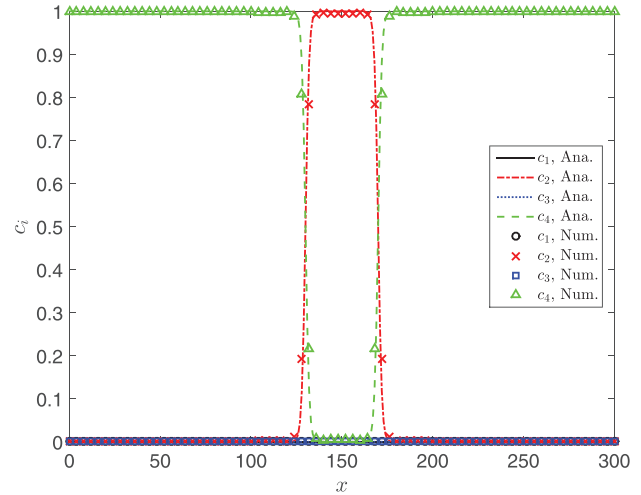


**FIG. 4.** A comparison of volume fractions obtained from the four-phase model with two phase disappeared and the theoretical solutions along the centerline ( $y = 50$ ,  $0 \leq x \leq 300$ ).

$$d = 2 \sqrt{\frac{A}{\sum_{i=1}^2 \frac{1}{\sin(\theta_i)} \left( \frac{\theta_i}{\sin \theta_i} - \cos \theta_i \right)}}, \quad (35)$$

where  $A$  is the lens area. With the aid of Eqs. (34) and (35), the heights can be determined as

$$h_i = \left( \frac{d}{2} \right) \frac{1 - \cos \theta_i}{\sin \theta_i}, \quad i = 1, 2. \quad (36)$$

We first study this problem as a three-phase system without gravity. In our simulations, the computational domain is chosen to be  $NX \times NY = 150 \times 150$ . The initial volume fractions are given by

$$c_1(x, y) = 0.5 + 0.5 \tanh \frac{2 \left[ R - \sqrt{(x - x_c)^2 + (y - y_c)^2} \right]}{D}, \quad (37a)$$

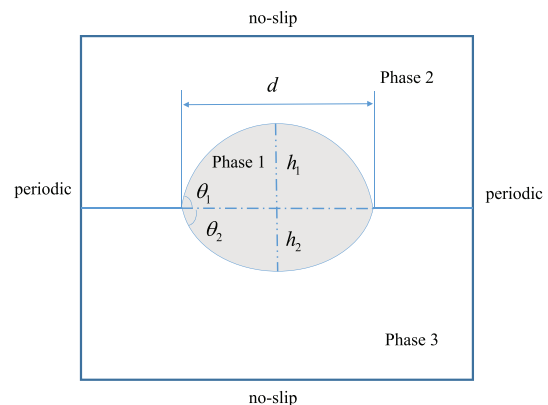


**FIG. 5.** The lens shape at the equilibrium state.

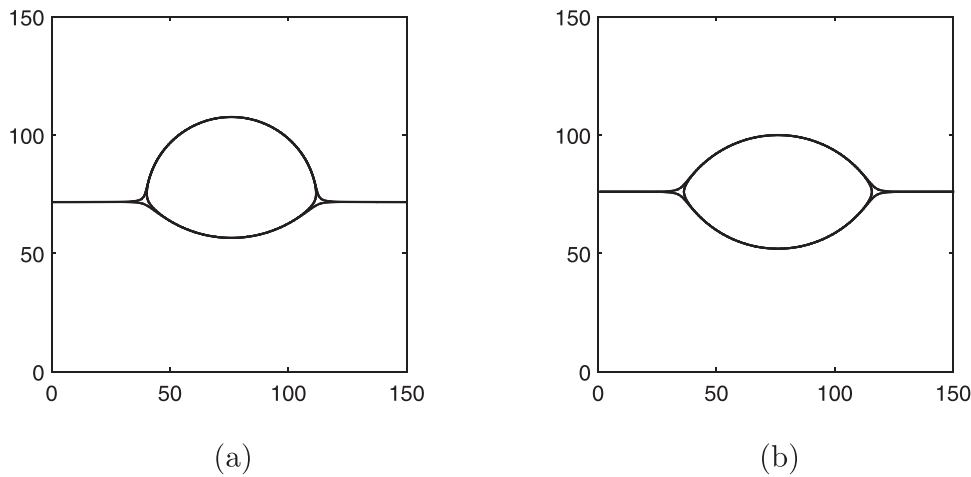


FIG. 6. The equilibrium droplet profiles of the lens with (a)  $\sigma_{12} : \sigma_{13} : \sigma_{23} = 1 : \frac{4}{3} : 1$  and (b)  $\sigma_{12} : \sigma_{13} : \sigma_{23} = 1 : 1 : 1$ .

$$c_2(x, y) = \max \left[ 0.5 + 0.5 \tanh \frac{2(y - y_c)}{D} - c_1(x, y), 0 \right], \quad (37b)$$

$$c_3(x, y) = 1.0 - c_1(x, y) - c_2(x, y), \quad (37c)$$

where  $(x_c, y_c)$  is the center of the circular droplet and  $R$  is the radius of the circular lens with  $R=30$ . Periodic boundary conditions are imposed on the right and left boundaries, and a no-slip boundary condition is enforced on the top and bottom walls. The density ratio of the three fluids is set to  $\rho_1 : \rho_2 : \rho_3 = 10 : 1 : 5$ , and the other physical parameters are set to  $D=3$ ,  $\tau_g = 0.8$ ,  $\omega_{ip} = \frac{1}{0.503} \delta_{ip}$ ,  $m_0 = 0.05$ ,  $\sigma_{12} : \sigma_{13} : \sigma_{23} = 1 : 1 : 1$  and  $1 : \frac{4}{3} : 1$ . The equilibrium droplet profiles of the liquid lens are plotted in Fig. 6. The system reaches distinct equilibrium states under different values of the surface tension ratio. Additionally, the shapes of the liquid interface are in good agreement with previous results.<sup>16,46,48,56</sup> To provide a quantitative analysis, we measured the contact angles ( $\theta_1$  and  $\theta_2$ ), length ( $d$ ), and heights ( $d_1$  and  $d_2$ ) of the lens. These are compared with the analytical solutions in Tables I and II. In Table I, the numerical results for the contact angles  $\theta_1$  and  $\theta_2$  are in good agreement with the analytical solutions, and the maximum relative errors are no more than 3.0%. From Table II, it is clear that the numerical solutions for the length  $d$  and height ( $h_1, h_2$ ) are consistent with the theoretical predictions, and the maximum relative errors of  $d, h_1$ , and  $h_2$  are less than 5.0%.

The spreading of a liquid lens can also be physically considered as a multiphase system consisting of four fluid components, in which one fluid is absent. We simulate this problem as a four-phase system in

which  $c_4 = 0$ . In this simulation,  $\rho_4 = 6$ ,  $\sigma_{i4} = 0.01$  ( $i = 1 - 4$ ), and the other parameters are the same as in the three-phase model. For both cases, the numerical results in Tables I and II are exactly the same, which indicates that the present LB model is reduction-consistent.

The effect of gravity on the equilibrium configurations is now considered. In this test, the gravitational acceleration  $g$  is assumed to be in the  $-y$  direction, and the magnitude of the gravitational acceleration varies from 0 to  $10^{-5}$ . The equilibrium configurations corresponding to these gravity values are simulated with all other physical parameters fixed. The computational domain is expanded to  $NX \times NY = 300 \times 150$  in this test because of the large deformation of the interface. The physical parameters are set to  $\rho_1 : \rho_2 : \rho_3 = 5 : 1 : 10$  for the three-phase model,  $\rho_1 : \rho_2 : \rho_3 : \rho_4 = 5 : 1 : 10 : 6$  for the four-phase model (fluid 4 absent),  $\sigma_{ij} = 0.01$  ( $i \neq j$ ),  $\omega_{ip} = \frac{1}{0.505} \delta_{ip}$ , and  $m_0 = 0.001$ .

According to the Langmuir-de Gennes theory,<sup>59,60</sup> when gravity is dominant, the droplet will form a puddle. The asymptotic puddle thickness  $H_a$  is determined by the strength of the gravitational acceleration, the three pairwise surface tensions, and the densities according to the following expression:

$$H_a = \sqrt{\frac{2(\sigma_{12} + \sigma_{13} - \sigma_{23})}{\frac{\rho_1}{\rho_3}(\rho_3 - \rho_1)g}}. \quad (38)$$

Figure 7 shows the asymptotic thickness as a function of gravity for the present three-phase model, four-phase model, and Langmuir-de

TABLE I. The equilibrium contact angles  $\theta_1$  and  $\theta_2$  with different surface tension ratios.

LB model	Surface tension ( $\sigma_{12} : \sigma_{13} : \sigma_{23}$ )	Numerical		Analytical		Relative errors	
		$\theta_1$	$\theta_2$	$\theta_1$	$\theta_2$	$\theta_1$	$\theta_2$
Three-phase model	1 : 1 : 1	59.7°	59.7°	60.0°	60.0°	0.5%	0.5%
	1 : $\frac{4}{3}$ : 1	84.3°	46.8°	83.6°	48.2°	0.8%	2.9%
Four-phase model	1 : 1 : 1	59.7°	59.7°	60.0°	60.0°	0.5%	0.5%
	1 : $\frac{4}{3}$ : 1	84.3°	46.8°	83.6°	48.2°	0.8%	2.9%



**TABLE II.** The equilibrium length  $d$  and height ( $h_1, h_2$ ) with different surface tension ratios.

LB model	Surface tension ( $\sigma_{12} : \sigma_{13} : \sigma_{23}$ )	Numerical			Analytical			Relative errors		
		$d$	$h_1$	$h_2$	$d$	$h_1$	$h_2$	$d$	$h_1$	$h_2$
Three-phase model	1 : 1 : 1	82.7	23.9	23.9	83.1	24.0	24.0	0.5%	0.4%	0.4%
	1 : $\frac{4}{3}$ : 1	74.2	34.9	16.1	75.5	33.8	16.9	1.7%	3.3%	4.7%
Four-phase model	1 : 1 : 1	82.7	23.9	23.9	83.1	24.0	24.0	0.5%	0.4%	0.4%
	1 : $\frac{4}{3}$ : 1	74.2	34.9	16.1	75.5	33.8	16.9	1.7%	3.3%	4.7%

Gennes theory.<sup>59,60</sup> When  $g$  is small, there is a large discrepancy between the numerical results and the Langmuir–de Gennes theory, because Langmuir–de Gennes theory is not valid for such values of  $g$ .<sup>2</sup> Actually, when  $g = 0$ , the numerical result for the asymptotic thickness ( $H_a = 47.8$ ) is very close to the theoretical value [ $h_1 + h_2 = 48.0$  in Table II, see Eq. (36)]. Similar results can be found in Ref. 45. As the gravitational acceleration increases ( $g \geq 2 \times 10^{-5}$ ), the numerical simulation results become closer to the Langmuir–de Gennes theory. Additionally, the results from the four-phase simulation almost exactly overlap with those from the three-phase simulation, suggesting that the present model preserves the reduction-consistency property.

### C. Kelvin–Helmholtz instability

We now consider the Kelvin–Helmholtz (KH) instability to illustrate the capacity of the present model to deal with complex interfacial dynamics. The KH instability typically occurs when there is velocity shear in a single continuous fluid, or where there is a velocity difference across the interface between fluids.<sup>62,63</sup> The KH instability phenomenon is an all-encompassing occurrence of fluid flow that is widespread in nature. From the waves of the ocean to the clouds in the sky, the KH instability is responsible for some of nature's most basic structures. Due to its importance, the KH instability has been widely investigated.<sup>58,64–69</sup> However, most numerical studies on the KH

instability are limited to two-phase systems.<sup>65–68</sup> In view of this, we attempt to simulate the KH instability of three immiscible incompressible fluids using the present LB model.

In this simulation, a square mesh of  $NX \times NY = 256 \times 256$  is adopted. The periodic boundary condition is applied in the  $x$  direction and the non-equilibrium extrapolation scheme<sup>70</sup> is used to treat the bottom and top boundaries. The initial setup is shown in Fig. 8. The initial volume fractions are given by

$$c_1(x, y) = 0.5 + 0.5 \tanh \frac{2(y - 2NY/3 - h)}{D}, \quad (39a)$$

$$c_2(x, y) = 0.5 + 0.5 \tanh \frac{2(y - NY/3 - h)}{D} - c_1(x, y), \quad (39b)$$

$$c_3(x, y) = 1.0 - c_1(x, y) - c_2(x, y), \quad (39c)$$

where  $h$  is a sinusoidal perturbation with  $h = 0.01NY \times \sin(\frac{4\pi x}{NX})$ . The initial distribution of the fluid velocity is set to<sup>69</sup>

$$u = U_0 + U_0 \left[ \tanh \frac{2(y - 2NY/3 - h)}{D} - \tanh \frac{2(y - NY/3 - h)}{D} \right], \quad (40a)$$

$$v = 0, \quad (40b)$$

where  $U_0$  is a constant velocity. In addition, the velocities for the bottom and top boundaries are fixed at  $u = U_0$  and  $v = 0$ . The KH instability is mainly characterized by the non-dimensional Reynolds number defined by  $Re = NY \times U_0 / \nu$ ; in this test,  $Re = 5000$ . The other parameters are set to  $\rho_1 : \rho_2 : \rho_3 = 0.98 : 0.99 : 1$ ,  $U_0 = 0.04$ ,

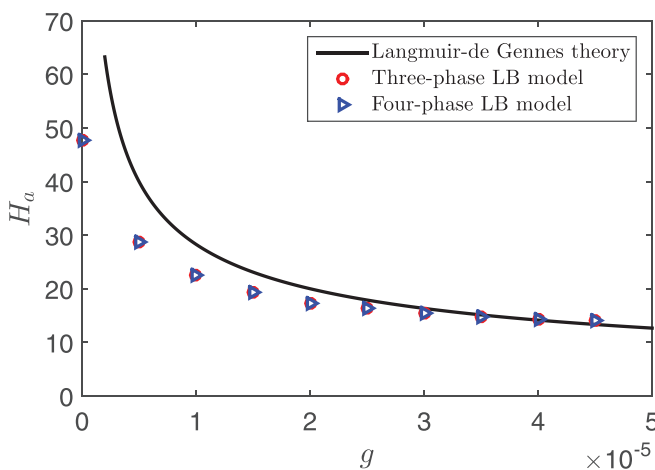


**FIG. 7.** A comparison of the asymptotic thickness  $H_a$  as a function of gravity  $g$  between the numerical results (by the three-phase and four-phase models) and the Langmuir–de Gennes theory.

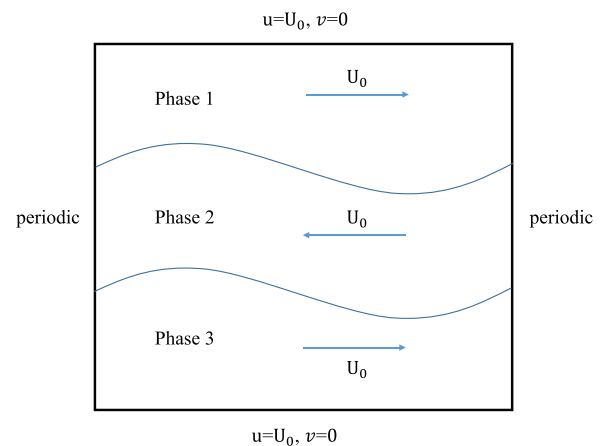


**FIG. 8.** The initial setup of the KH instability test.

$D = 3$ ,  $\omega_{ip} = \frac{1}{0.505} \delta_{ip}$ ,  $m_0 = 0.0002$ , and  $\sigma_{12} = \sigma_{13} = \sigma_{23} = 0.0001$ . Figure 9 shows the evolution of the density with two sinusoidal interface perturbations. Because of the shear stress effect, the upper and lower interfaces gradually curl up, forming the shape of billows. This curling of the interface becomes more severe with time. This phenomenon can be explained by the accumulation of vorticity. As shown in Fig. 10, the vorticity accumulates in the billow cores, resulting in the formation of thin braids and cores of vorticity.<sup>69</sup> As a result, vortices form and gradually grow over time. The current simulation results are compared with those in Ref. 58 (see Figs. 9 and 10), and there is good agreement between the two.

#### D. Dynamics of droplets in a four-phase system

The rising and falling of droplets are very common phenomena in nature and in engineering applications such as in inkjet printing, microreactors, and kitchens.<sup>2,71,72</sup> To demonstrate the capability of the present LB model to handle such complex problems, we now consider the dynamics of droplets in a system composed of four immiscible incompressible fluids under gravity/buoyancy. The setting of this problem is shown in Fig. 11, where the rectangular domain is fixed to be  $NY \times NX = 480 \times 160$ . At  $t = 0$ , the top part of the domain is filled with phase 2, and the bottom part is full of phase 3. Two circular droplets of radius  $R = 20$  centered at  $(NX/2, NY/8)$  (phase 1) and  $(NX/2, 7NY/8)$  (phase 4) start to move under gravity/buoyancy simultaneously. The initial volume fractions are given by

$$c_1(x, y) = 0.5 + 0.5 \tanh \frac{2 \left[ R - \sqrt{(x - x_{c_1})^2 + (y - y_{c_1})^2} \right]}{D}, \quad (41a)$$

$$c_4(x, y) = 0.5 + 0.5 \tanh \frac{2 \left[ R - \sqrt{(x - x_{c_2})^2 + (y - y_{c_2})^2} \right]}{D}, \quad (41b)$$

$$c_2(x, y) = \left[ 0.5 + 0.5 \tanh \frac{2(y - y_0)}{D} \right] \times [1.0 - c_4(x, y)] \quad (41c)$$

$$c_3(x, y) = 1.0 - c_1(x, y) - c_2(x, y) - c_4(x, y), \quad (41d)$$

where  $(x_{c_1}, y_{c_1})$  and  $(x_{c_2}, y_{c_2})$  are the centers of the two droplets and  $y_0 = \frac{1}{2}NY$  is the initial position of the interface between phases 3 and 4. In this test, periodic boundary conditions are imposed on the right and left boundaries, while the no-slip boundary condition is imposed on the top and bottom walls. Different values of the surface tensions  $\sigma_{23}$  are considered. The physical parameters are set to  $\rho_1 : \rho_2 : \rho_3 : \rho_4 = 1 : 3 : 4 : 6$ ,  $\sigma_{12} = \sigma_{13} = \sigma_{14} = \sigma_{24} = \sigma_{34} = 0.01$ ,  $\sigma_{23} = 0.001, 0.01, 0.03$ ,  $m_0 = 0.01$ ,  $D = 3$ ,  $g = 2 \times 10^{-5}$ ,  $\tau_g = 0.8$ , and  $\omega_{ip} = \frac{1}{0.505} \delta_{ip}$ . Since phase 1 is lighter than phase 3 and phase 4 is heavier than phase 2, the droplet of phase 1 should be rising while phase 4 droplet should be falling down. Figure 12 shows a temporal sequence of snapshots of the fluid interface for various values of  $\sigma_{23}$ . For  $\sigma_{23} = 0.001$ , phases 1 and 4 undergo significant deformation under the action of surface tension and gravity, and the interface between phases 2 and 3 becomes curved due to the effect of the droplets on both sides ( $t = 16.97$ , where the time has been non-dimensionalized by  $t = \frac{t_l}{\sqrt{\frac{2R}{g}}}$  with  $t_l$  being the lattice time). After that,

phase 1 continues to rise, producing a severe deformation of phase 4 and in the interface between phases 2 and 3 ( $t = 21.21$ ). Finally, phase

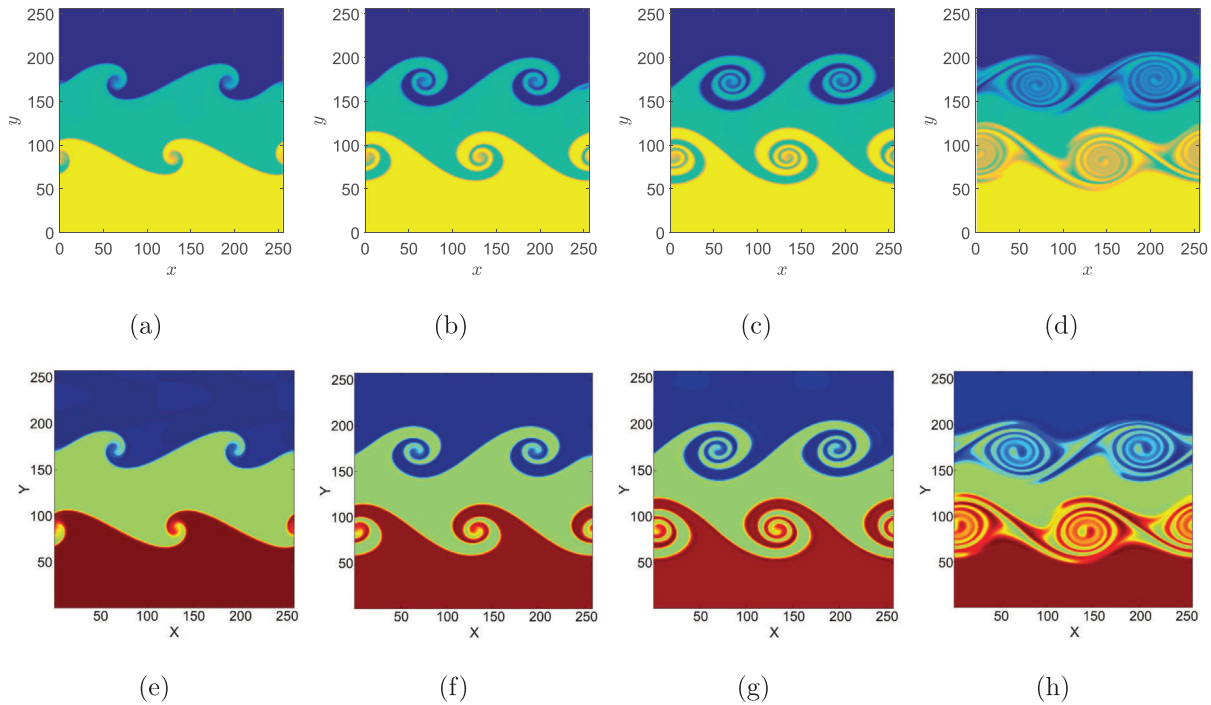


**FIG. 9.** The density at  $t = 2000$ ,  $t = 3000$ ,  $t = 4000$ ,  $t = 9000$ . [(a)–(d) present LB model and (e)–(h) LB model in the previous work.<sup>58</sup>] Reproduced with permission from Phys. Rev. E 93, 013308 (2016). Copyright 2016 American Physical Society.

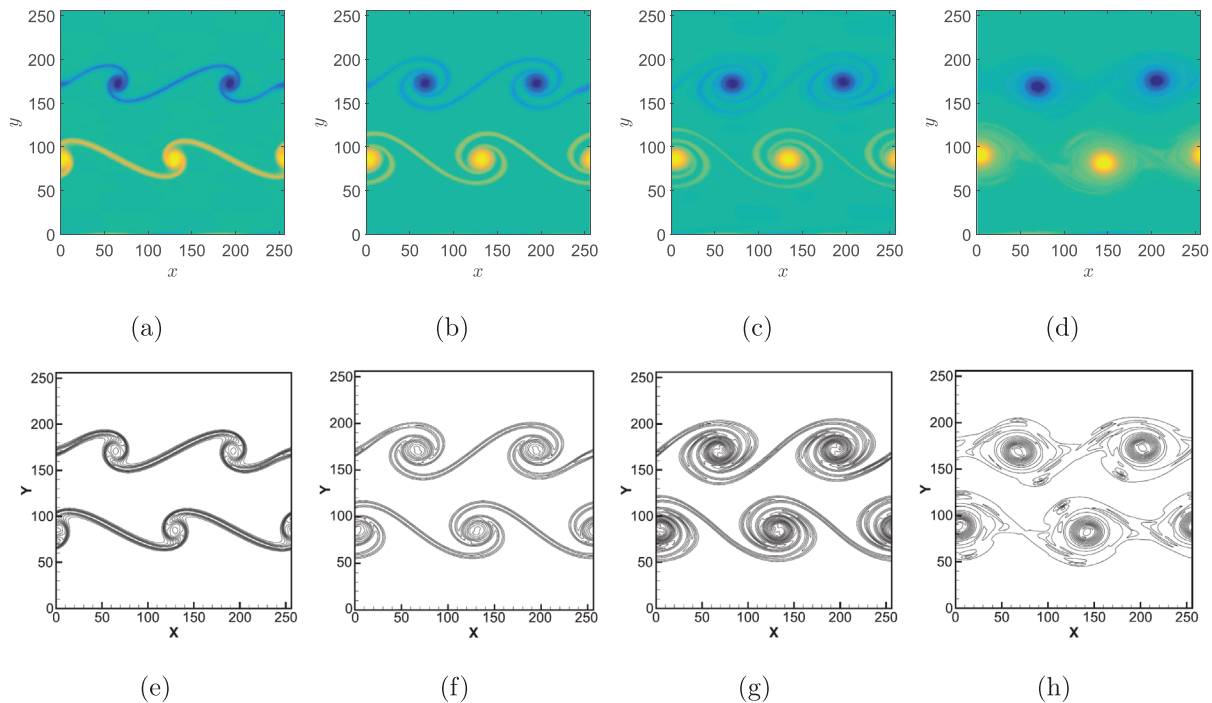


**FIG. 10.** The vorticity field at  $t = 2000$ ,  $t = 3000$ ,  $t = 4000$ ,  $t = 9000$ . [(a)–(d) Present LB model and (e)–(h) LB model in the previous work.<sup>58</sup>]

4 breaks into two sub-droplets, and phase 1 departs from the interface ( $t = 28.28$ – $42.43$ ).

An increase in the surface tension  $\sigma_{23}$  makes the deformation of the interface between phases 2 and 3 less obvious at the same moment (see Fig. 12), and it becomes increasingly difficult for phase 1 to pass through the interface. This is because an increase in  $\sigma_{23}$  means that

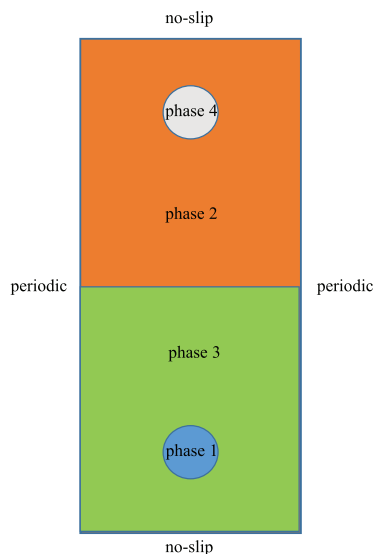


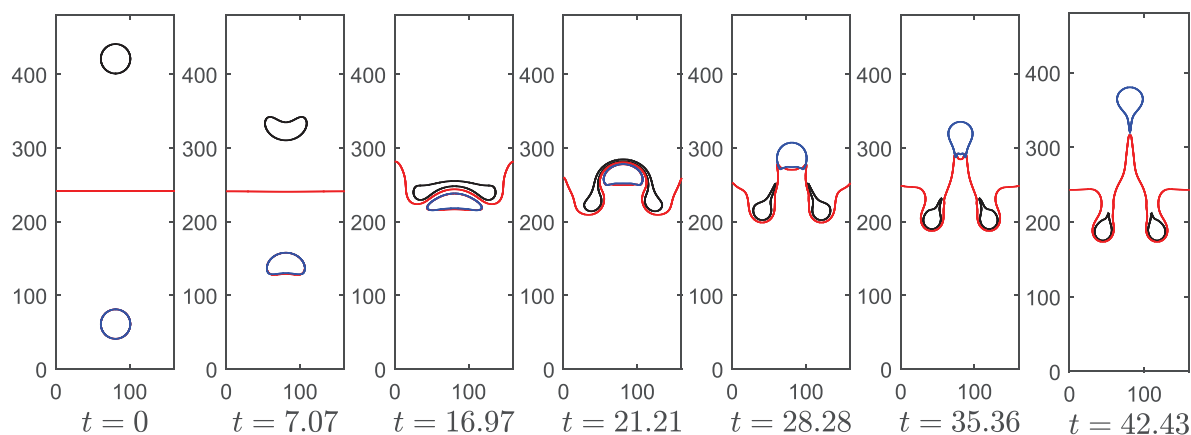
**FIG. 11.** Initial configuration of droplet collision in a four-phase system.

more energy is needed to produce the same degree of deformation of the interface between phases 2 and 3. As illustrated in Fig. 12, the present numerical results meet our expectations.

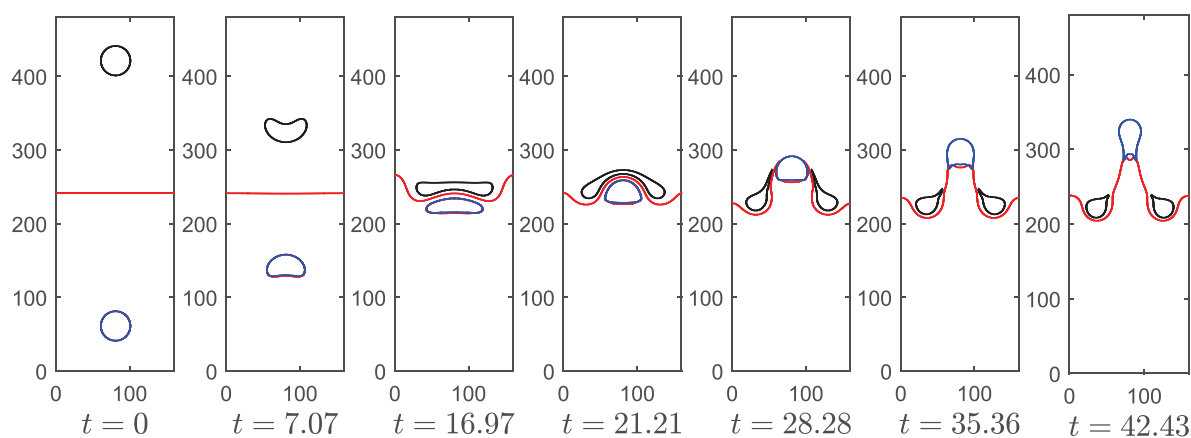
We now examine the dynamical features of this four-phase flow by investigating the velocity distributions. Figure 13 shows a temporal sequence of snapshots of the velocity fields at the same times as the images in Fig. 12. From Fig. 13(a), we can observe that, prior to the impact on the surface between phases 2 and 3 ( $t = 7.07$ – $16.97$ ), phases 1 and 4 induce a velocity field, forming two pair of vortices near the shoulders of these phases. At the time  $t = 21.21$ , only a pair of significant vortices is observed. Under their action, phase 1 continues to rise, while phase 4 breaks into two sub-droplets. Subsequently, phase 1 crosses the interface between phases 2 and 3 and induces a new pair of vortices ( $t = 28.28$ – $42.43$ ). At the same time, the vortices around the sub-droplets of phase 4 gradually weaken. Finally, the system reaches a relatively stable state. With an increase in surface tension  $\sigma_{23}$ , we find that the velocity distribution at the same moment ( $t > 16.97$ ) exhibits a smaller gradient. This is because greater surface tension at the interface hinders the movement of droplets on either side of the interface, so the droplet moves more smoothly. From the above discussion, it can be concluded that the present LB model works well in simulating complicated dynamical problems in a four-phase system.

## V. CONCLUSIONS

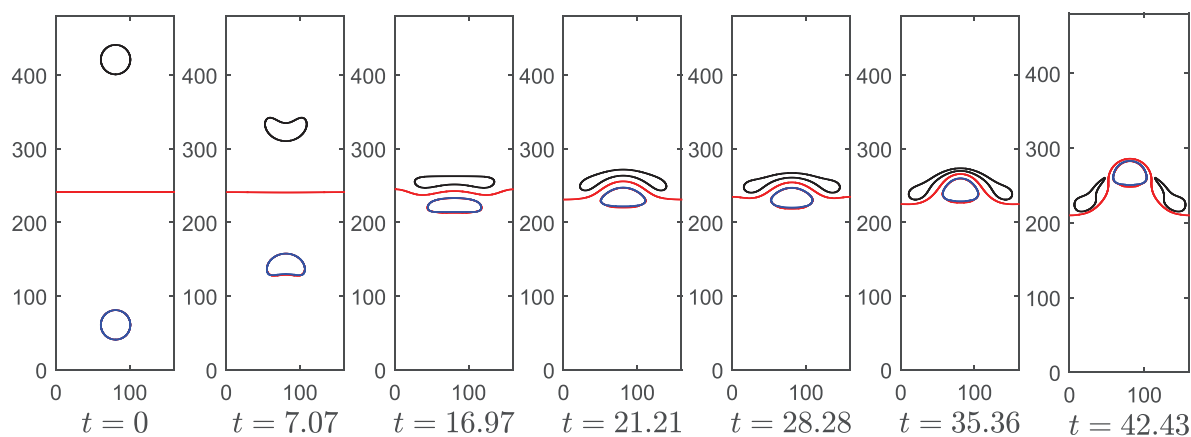
In this paper, we have developed an efficient and accurate phase-field-based LB model for multiphase flows consisting of  $N$  ( $N \geq 2$ ) immiscible incompressible fluids. A new LB equation for the phase field governed by  $N$  coupled C–H equations was first proposed. In particular, the mobility  $m_{ij}$  depends on the volume fraction. To solve this



(a)



(b)



(c)

**FIG. 12.** Time evolution of the fluid interfaces at  $t = 0$ ,  $t = 7.07$ ,  $t = 16.97$ ,  $t = 21.21$ ,  $t = 28.28$ ,  $t = 35.36$ ,  $t = 42.43$ , (a)  $\sigma_{23} = 0.001$ , (b)  $\sigma_{23} = 0.01$ , and (c)  $\sigma_{23} = 0.03$ .

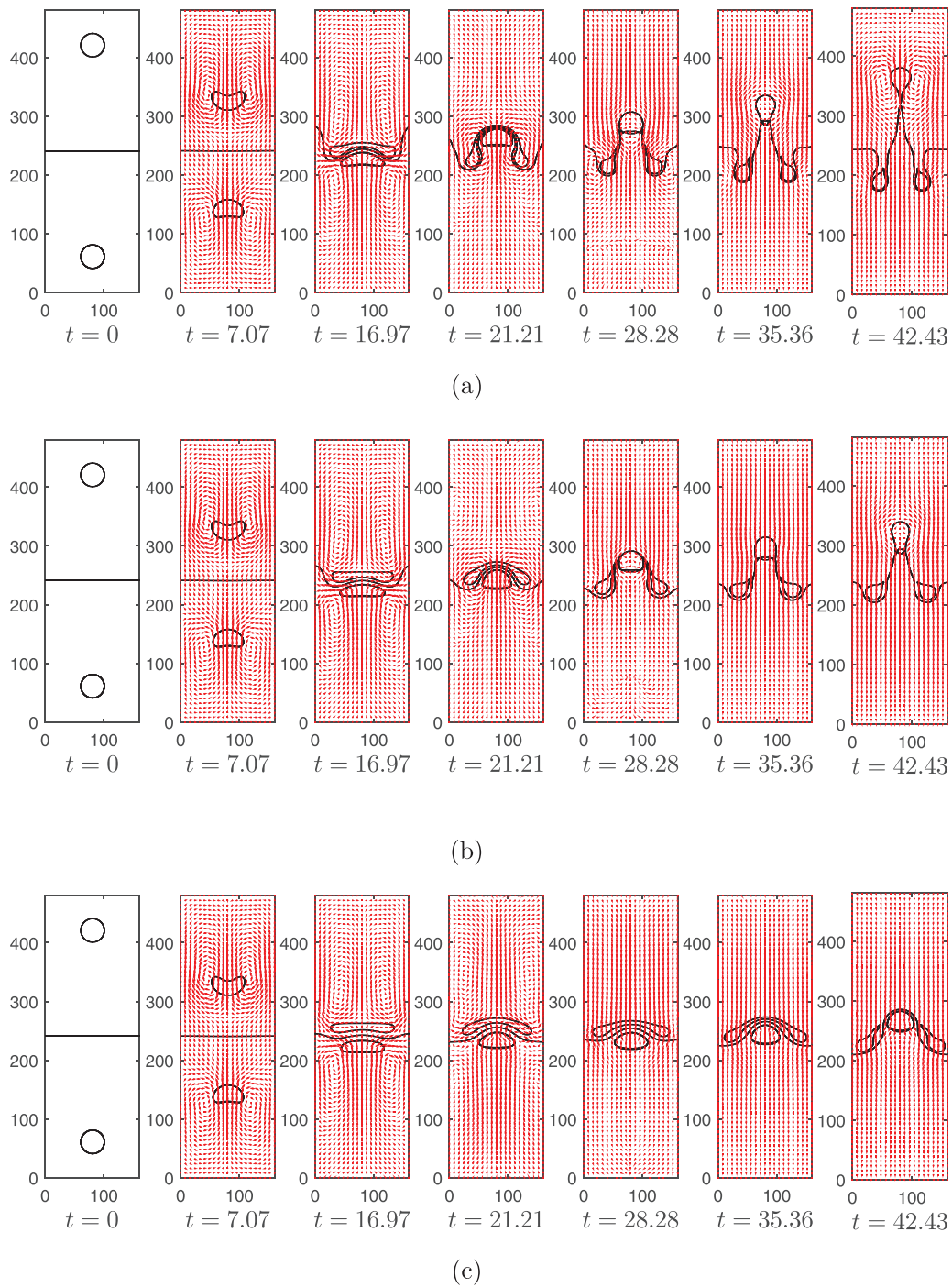


**FIG. 13.** Evolution of the velocity fields at  $t = 0$ ,  $t = 7.07$ ,  $t = 16.97$ ,  $t = 21.21$ ,  $t = 28.28$ ,  $t = 35.36$ ,  $t = 42.43$ , (a)  $\sigma_{23} = 0.001$ , (b)  $\sigma_{23} = 0.01$ , and (c)  $\sigma_{23} = 0.03$ .

problem, some extra collision operators were introduced to model the cross-diffusion terms; simultaneously, proper auxiliary source terms were constructed to derive the correct macroscopic equations. Note that, compared with previous LB models for multiphase flows, there is

no need to calculate the chemical potential gradient in the current LB model. In addition, another LB equation was adopted for the flow field. Direct Taylor expansion analysis showed that the present LB model derives the macroscopic equations correctly.



Four classical problems were used to demonstrate the capability of the LB model. In the tests considering static droplets and the spreading of a liquid lens, the present LB model was found to capture the interface accurately, and the numerical results were in good agreement with analytical solutions. These two examples also illustrated that the present LB model has the reduction-consistency property. We then studied the KH instability of three immiscible incompressible fluids, and compared the numerical results with those of Liang *et al.*<sup>58</sup> Good agreement was observed between the two sets of results. Finally, the dynamics of droplets in a four-phase system were investigated to demonstrate the capability of the present LB model to handle complex  $N$ -phase ( $N > 3$ ) flow problems. The results show that the surface tension has a significant influence on the dynamic behavior of droplets. All the numerical results presented here indicate that the LB model established in this study is accurate and efficient for multiphase flows.

## ACKNOWLEDGMENTS

This work was financially supported by the National Natural Science Foundation of China (Grant Nos. 12072127 and 51836003).

## AUTHOR DECLARATIONS

### Conflict of Interest

There are no conflicts of interest.

## DATA AVAILABILITY

The data that support the findings of this study are available within the article.

## REFERENCES

- A. Maghzi, S. Mohammadi, M. H. Ghazanfari, R. Kharrat, and M. Masihi, "Monitoring wettability alteration by silica nanoparticles during water flooding to heavy oils in five-spot systems: A pore-level investigation," *Exp. Therm. Fluid Sci.* **40**, 168–176 (2012).
- S. Dong, "An efficient algorithm for incompressible  $N$ -phase flows," *J. Comput. Phys.* **276**, 691–728 (2014).
- F. Boyer, C. Lapuerta, S. Minjeaud, B. Piar, and M. Quintard, "Cahn-Hilliard/Navier-Stokes model for the simulation of three-phase flows," *Transp. Porous Media* **82**, 463–483 (2010).
- A. S. Utada, E. Lorenceau, D. R. Link, P. D. Kaplan, H. A. Stone, and D. A. Weitz, "Monodisperse double emulsions generated from a microcapillary device," *Science* **308**, 537–541 (2005).
- A. Tiribocchi, A. Montessori, M. Lauricella, F. Bonaccorso, S. Succi, S. Aime, M. Milani, and D. A. Weitz, "The vortex-driven dynamics of droplets within droplets," *Nat. Commun.* **12**, 82 (2021).
- J. Guzowski and P. Garstecki, "Droplet clusters: Exploring the phase space of soft mesoscale atoms," *Phys. Rev. Lett.* **114**, 188302 (2015).
- Y. Yu, H. H. Liu, D. Liang, and Y. H. Zhang, "A versatile lattice Boltzmann model for immiscible ternary fluid flows," *Phys. Fluids* **31**, 012108 (2019).
- C. Hirt and B. Nichols, "Volume of fluid (VOF) method for the dynamics of free boundaries," *J. Comput. Phys.* **39**, 201–225 (1981).
- D. Gueyffier, J. Li, A. Nadim, R. Scardovelli, and S. Zaleski, "Volume-of-fluid interface tracking with smoothed surface stress methods for three-dimensional flows," *J. Comput. Phys.* **152**, 423–456 (1999).
- S. Osher and J. A. Sethian, "Fronts propagating with curvature-dependent speed: Algorithms based on Hamilton-Jacobi formulations," *J. Comput. Phys.* **79**, 12–49 (1988).
- N. Nangia, B. E. Griffith, N. A. Patankar, and A. P. S. Bhalla, "A robust incompressible Navier-Stokes solver for high density ratio multiphase flows," *J. Comput. Phys.* **390**, 548–594 (2019).
- S. O. Unverdi and G. Tryggvason, "A front-tracking method for viscous, incompressible, multi-fluid flows," *J. Comput. Phys.* **100**, 25–37 (1992).
- L. Rayleigh, "XX. On the theory of surface forces. II. Compressible fluids," *London, Edinburgh, Dublin Philos. Mag. J. Sci.* **33**, 209–220 (1892).
- H. Garcke, B. Nestler, and B. Stoth, "A multiphase field concept: Numerical simulations of moving phase boundaries and multiple junctions," *SIAM J. Appl. Math.* **60**, 295–315 (1999).
- J. Kim, K. Kang, and J. Lowengrub, "Conservative multigrid methods for ternary Cahn-Hilliard systems," *Comm. Math. Sci.* **2**, 53–77 (2004).
- F. Boyer and C. Lapuerta, "Study of a three component Cahn-Hilliard flow model," *ESAIM: Math. Modell. Numer. Anal.* **40**, 653–687 (2006).
- J. Kim, "Phase field computations for ternary fluid flows," *Comput. Methods Appl. Mech. Eng.* **196**, 4779–4788 (2007).
- Z. Huang, G. Lin, and A. M. Ardekani, "A consistent and conservative model and its scheme for  $N$ -phase- $M$ -component incompressible flows," *J. Comput. Phys.* **434**, 110229 (2021).
- X.-D. Niu, Y. Li, Y.-R. Ma, M.-F. Chen, X. Li, and Q.-Z. Li, "A mass-conserving multiphase lattice Boltzmann model for simulation of multiphase flows," *Phys. Fluids* **30**, 013302 (2018).
- G. Q. Chen, X. Huang, A. M. Zhang, and S. P. Wang, "Simulation of three-dimensional bubble formation and interaction using the high-density-ratio lattice Boltzmann method," *Phys. Fluids* **31**, 027102 (2019).
- E. Ezzatneshan, "Study of surface wettability effect on cavitation inception by implementation of the lattice Boltzmann method," *Phys. Fluids* **29**, 113304 (2017).
- X. Liu, Z. H. Chai, and B. C. Shi, "A phase-field-based lattice Boltzmann modeling of two-phase electrohydrodynamic flows," *Phys. Fluids* **31**, 092103 (2019).
- A. K. Gunstensen, D. H. Rothman, S. Zaleski, and G. Zanetti, "Lattice Boltzmann model of immiscible fluids," *Phys. Rev. A* **43**, 4320 (1991).
- X. Shan and H. Chen, "Simulation of nonideal gases and liquid-gas phase transitions by the lattice Boltzmann equation," *Phys. Rev. E* **49**, 2941 (1994).
- M. Swift, W. Osborn, and J. Yeomans, "Lattice Boltzmann simulation of non-ideal fluids," *Phys. Rev. Lett.* **75**, 830 (1995).
- X. He, S. Chen, and R. Zhang, "A lattice Boltzmann scheme for incompressible multiphase flow and its application in simulation of Rayleigh-Taylor instability," *J. Comput. Phys.* **152**, 642–663 (1999).
- Y. Wang, C. Shu, H. Huang, and C. Teo, "Multiphase lattice Boltzmann flux solver for incompressible multiphase flows with large density ratio," *J. Comput. Phys.* **280**, 404–423 (2015).
- H. Liang, B. C. Shi, Z. L. Guo, and Z. H. Chai, "Phase-field-based multiple-relaxation-time lattice Boltzmann model for incompressible multiphase flows," *Phys. Rev. E* **89**, 053320 (2014).
- A. Fakhari and D. Bolster, "Diffuse interface modeling of three-phase contact line dynamics on curved boundaries: A lattice Boltzmann model for large density and viscosity ratios," *J. Comput. Phys.* **334**, 620–638 (2017).
- Z. Chai, D. Sun, H. Wang, and B. Shi, "A comparative study of local and non-local Allen-Cahn equations with mass conservation," *Int. J. Heat Mass Transfer* **122**, 631–642 (2018).
- H. Wang, X. Yuan, H. Liang, Z. Chai, and B. Shi, "A brief review of the phase-field-based lattice Boltzmann method for multiphase flows," *Capillarity* **2**, 33–52 (2019).
- X. Zhang, H. Liu, and J. Zhang, "A new capillary force model implemented in lattice Boltzmann method for gas-liquid-solid three-phase flows," *Phys. Fluids* **32**, 103301 (2020).
- A. Lamura, G. Gonnella, and J. Yeomans, "A lattice Boltzmann model of ternary fluid mixtures," *Europhys. Lett.* **45**, 314 (1999).
- H. Chen, B. M. Boghosian, P. V. Coveney, and M. Nekovee, "A ternary lattice Boltzmann model for amphiphilic fluids," *Proc. R. Soc. London, Ser. A* **456**, 2043–2057 (2000).
- S. Leclaire, M. Reggio, and J. Trepanier, "Progress and investigation on lattice Boltzmann modeling of multiple immiscible fluids or components with variable density and viscosity ratios," *J. Comput. Phys.* **246**, 318–342 (2013).
- J. Bao and L. Schaefer, "Lattice Boltzmann equation model for multi-component multi-phase flow with high density ratios," *Appl. Math. Modell.* **37**, 1860–1871 (2013).
- C. Semprebon, T. Krüger, and H. Kusumaatmaja, "Ternary free-energy lattice Boltzmann model with tunable surface tensions and contact angles," *Phys. Rev. E* **93**, 033305 (2016).



- <sup>38</sup>Y. Fu, S. Zhao, L. Bai, Y. Jin, and Y. Cheng, "Numerical study of double emulsion formation in microchannels by a ternary lattice Boltzmann method," *Chem. Eng. Sci.* **146**, 126–134 (2016).
- <sup>39</sup>Y. Shi, G. Tang, and Y. Wang, "Simulation of three-component fluid flows using the multiphase lattice Boltzmann flux solver," *J. Comput. Phys.* **314**, 228–243 (2016).
- <sup>40</sup>R. H. H. Abadi, M. H. Rahimian, and A. Fakhari, "Conservative phase-field lattice-Boltzmann model for ternary fluids," *J. Comput. Phys.* **374**, 668–691 (2018).
- <sup>41</sup>R. H. H. Abadi, A. Fakhari, and M. H. Rahimian, "Numerical simulation of three-component multiphase flows at high density and viscosity ratios using lattice Boltzmann methods," *Phys. Rev. E* **97**, 033312 (2018).
- <sup>42</sup>M. Wöhrwag, C. Semperebon, A. M. Moqaddam, I. Karlin, and H. Kusumaatmaja, "Ternary free-energy entropic lattice Boltzmann model with a high density ratio," *Phys. Rev. Lett.* **120**, 234501 (2018).
- <sup>43</sup>Y. Hu, D. Li, and Q. He, "Generalized conservative phase field model and its lattice Boltzmann scheme for multicomponent multiphase flows," *Int. J. Multiphase Flow* **132**, 103432 (2020).
- <sup>44</sup>L. Zheng, S. Zheng, and Q. Zhai, "Reduction-consistent phase-field lattice Boltzmann equation for N immiscible incompressible fluids," *Phys. Rev. E* **101**, 043302 (2020).
- <sup>45</sup>S. Dong, "Multiphase flows of N immiscible incompressible fluids: A reduction-consistent and thermodynamically-consistent formulation and associated algorithm," *J. Comput. Phys.* **361**, 1–49 (2018).
- <sup>46</sup>L. Zheng and S. Zheng, "Phase-field-theory-based lattice Boltzmann equation method for N immiscible incompressible fluids," *Phys. Rev. E* **99**, 063310 (2019).
- <sup>47</sup>L. Zheng, S. Zheng, and Q. Zhai, "Reduction-consistent Cahn-Hilliard theory based lattice Boltzmann equation method for N immiscible incompressible fluids," *Physica A* **574**, 126015 (2021).
- <sup>48</sup>X. L. Yuan, H. Liang, Z. H. Chai, and B. C. Shi, "Phase-field-based lattice Boltzmann model for immiscible incompressible N-phase flows," *Phys. Rev. E* **101**, 063310 (2020).
- <sup>49</sup>Z. Chai, X. Guo, L. Wang, and B. Shi, "Maxwell-Stefan-theory-based lattice Boltzmann model for diffusion in multicomponent mixtures," *Phys. Rev. E* **99**, 023312 (2019).
- <sup>50</sup>C. Zhan, Z. Chai, and B. Shi, "A lattice Boltzmann model for the coupled cross-diffusion-fluid system," *Appl. Math. Comput.* **400**, 126105 (2021).
- <sup>51</sup>H. H. Liu, A. J. Valocchi, Y. H. Zhang, and Q. J. Kang, "Lattice Boltzmann phase-field modeling of thermocapillary flows in a confined microchannel," *J. Comput. Phys.* **256**, 334–356 (2014).
- <sup>52</sup>Y. H. Qian, D. d'Humières, and P. Lallemand, "Lattice BGK models for Navier-Stokes equation," *Europhys. Lett.* **17**, 479 (1992).
- <sup>53</sup>Z. Guo, C. Zheng, and B. Shi, "Discrete lattice effects on the forcing term in the lattice Boltzmann method," *Phys. Rev. E* **65**, 046308 (2002).
- <sup>54</sup>J. Kim, "A continuous surface tension force formulation for diffuse-interface models," *J. Comput. Phys.* **204**, 784–804 (2005).
- <sup>55</sup>Y. Zu and S. He, "Phase-field-based lattice Boltzmann model for incompressible binary fluid systems with density and viscosity contrasts," *Phys. Rev. E* **87**, 043301 (2013).
- <sup>56</sup>K. A. Smith, F. J. Solis, and D. L. Chopp, "A projection method for motion of triple junctions by level sets," *Interfaces Free Boundaries* **4**, 263–276 (2002).
- <sup>57</sup>T. J. Spencer, I. Halliday, and C. M. Care, "Lattice Boltzmann equation method for multiple immiscible continuum fluids," *Phys. Rev. E* **82**, 066701 (2010).
- <sup>58</sup>H. Liang, B. C. Shi, and Z. H. Chai, "Lattice Boltzmann modeling of three-phase incompressible flows," *Phys. Rev. E* **93**, 013308 (2016).
- <sup>59</sup>I. Langmuir, "Oil lenses on water and the nature of monomolecular expanded films," *J. Chem. Phys.* **1**, 756–776 (1933).
- <sup>60</sup>P. de Gennes, F. Brochard-Wyart, and D. Quéré, *Capillarity and Wetting Phenomena: Drops, Bubbles, Pearls, Waves* (Springer, New York, 2004).
- <sup>61</sup>J. S. Rawlinson and B. Widom, *Molecular Theory of Capillarity* (Clarendon Press, Oxford, 1982).
- <sup>62</sup>W. S. Thomson, "Hydrokinetic solutions and observations," *Philos. Mag.* **42**, 362–377 (1871).
- <sup>63</sup>R. Govindarajan and K. C. Sahu, "Instabilities in viscosity-stratified flow," *Annu. Rev. Fluid Mech.* **46**, 331–353 (2014).
- <sup>64</sup>S. Chandrasekhar, *Hydrodynamic and Hydromagnetic Stability* (Clarendon Press, Oxford, 1961).
- <sup>65</sup>T. Funada and D. D. Joseph, "Viscous potential flow analysis of Kelvin-Helmholtz instability in a channel," *J. Fluid Mech.* **445**, 263–283 (2001).
- <sup>66</sup>D. I. Pullin, "Numerical studies of surface-tension effects in nonlinear Kelvin-Helmholtz and Rayleigh-Taylor instability," *J. Fluid Mech.* **119**, 507–532 (1982).
- <sup>67</sup>R. D. Moser and M. M. Rogers, "The three-dimensional evolution of a plane mixing layer: Pairing and transition to turbulence," *J. Fluid Mech.* **247**, 275–320 (1993).
- <sup>68</sup>R. Zhang, X. He, G. D. Doolen, and S. Chen, "Surface tension effects on two-dimensional two-phase Kelvin-Helmholtz instabilities," *Adv. Water Res.* **24**, 461–478 (2001).
- <sup>69</sup>H. G. Lee and J. Kim, "Two-dimensional Kelvin-Helmholtz instabilities of multi-component fluids," *Eur. J. Mech. B-Fluid* **49**, 77–88 (2015).
- <sup>70</sup>Z. L. Guo, C. G. Zheng, and B. C. Shi, "An extrapolation method for boundary conditions in lattice Boltzmann method," *Phys. Fluids* **14**, 2007–2010 (2002).
- <sup>71</sup>J. Qian and C. K. Law, "Regimes of coalescence and separation in droplet collision," *J. Fluid Mech.* **331**, 59–80 (1997).
- <sup>72</sup>H. Hinterbichler, C. Planchette, and G. Brenn, "Ternary drop collisions," *Exp. Fluids* **56**, 190 (2015).